Catalysis Today 164 (2011) 214–220

Contents lists available at ScienceDirect

Catalysis Today

journal homepage: www.elsevier.com/locate/cattod

Propane dehydrogenation over Pt–Sn/Rare-earth-doped Al_2O_3: Influence of La, Ce, or Y on the formation and stability of Pt–Sn alloys

Bao Khanh Vu[a], Myoung Bok Song[a], In Young Ahn[b], Young-Woong Suh[b], Dong Jin Suh[b], Won-IL Kim[c], Hyoung-Lim Koh[c], Young Gyo Choi[c], Eun Woo Shin[a,*]

[a] School of Chemical Engineering and Bioengineering, University of Ulsan, Daehakro 102, Nam-gu, Ulsan 680-749, South Korea
[b] Korea Institute of Science and Technology, Wolsong-gil 5, Seongbuk-gu, Seoul 136-791, South Korea
[c] Production R&D Center, Hyosung Co., Hogye-dong, Dongan-gu, Anyang, GyeoungGi 431-080, South Korea

ARTICLE INFO

Article history:
Available online 3 November 2010

Keywords:
Propane dehydrogenation
Rare-earth-doped alumina
Bimetallic catalyst
Catalytic deactivation
Pt–Sn alloy

ABSTRACT

In this study, La, Ce, or Y has been successfully incorporated into the γ-Al_2O_3 framework to improve the Pt dispersion. Moreover, La and Y formed a dispersed phase, while a large portion of Ce constituted a separate phase on the Al_2O_3 support in the form of CeO_2. The formation and stability of the Pt–Sn alloy in the catalysts were remarkably influenced by the addition of La, Ce, or Y. Compared to pure Al_2O_3 supports, La-doped Al_2O_3 promoted the formation of PtSn, while Ce- and Y-doped Al_2O_3 promoted the formation of $PtSn_2$ alloy on reduced catalysts. However, the stability of Pt–Sn alloy during the reaction exhibited different tolerances according to the catalyst used. Compared to those of the Pt–Sn/Al and Pt–Sn/Y–Al catalysts, Pt–Sn/La–Al and Pt–Sn/Ce–Al catalysts showed superior catalytic performances and stabilities because of the lower coke contents, higher stabilities of PtSn and $PtSn_2$ alloys, and smaller losses of Pt dispersion. This study suggests that the type and stability of Pt–Sn alloy formed on the Pt–Sn/support catalyst, which determined the catalytic performance and stability, were remarkably influenced by the support.

1. Introduction

Pt/Al_2O_3 catalysts are active in propane dehydrogenation; however, monometallic Pt catalyst systems exhibit quick catalyst deactivation under high reaction temperatures. To improve the catalytic performances and stabilities of Pt/Al_2O_3 catalysts, the most frequently applied promoter is tin, and its role was proposed to modify the catalytic properties of Pt via electronic and ligand effects [1,2]. However, $Pt–Sn/Al_2O_3$ catalysts must undergo continuous or frequent regenerations to restore the catalytic activity as deactivation due to coking cannot be completely eliminated [3]. Consequently, other promoters, including alkali metals (Li, K, Na), Zn, and rare earth metals (La, Ce, Y), have been added to $Pt–Sn/Al_2O_3$ catalysts to enhance the tolerance against catalyst deactivation. The primary roles of these promoters are to improve the thermal stabilities of supports and to modify the acidic/basic properties of supports and metal-support interactions [4–9]. $ZnAl_2O_4$ or $MgAl_2O_4$ was also used as supports due to their neutral characteristics and very high thermal stabilities [10,11].

The accurate nature of the Pt–Sn bimetallic systems is complicated and remains a matter of debate. The natures of the Pt–Sn bimetallic systems depend on several factors such as supports [12,13], method of catalytic preparation [14–16], metallic precursors [17,18], sequence of preparation [16,19], metal loading [16] and pretreatment conditions [20]. Due to the complexity of Pt–Sn bimetallic systems, there is no single adequate model to describe the sophisticated characterization data [21].

Although La, Ce, and Y have been used as promoters to enhance the stabilities of $Pt–Sn/Al_2O_3$ catalysts, the role of La-, Ce-, and Y-doped Al_2O_3 in the formation and stability of Pt–Sn alloy has been not examined. In this study, Pt–Sn catalysts supported on Al_2O_3 and on La-, Ce-, and Y-doped Al_2O_3 were prepared and used for propane dehydrogenation. Influences of La-, Ce-, and Y-doped Al_2O_3 supports on the formations and stabilities of Pt–Sn alloys in propane dehydrogenation were investigated. To this end, the prepared catalysts were characterized using N_2 sorption, NMR, CO chemisorption, TPR, XRD, HRTEM, XPS, and TGA. Specifically, the XRD measurements were used as a primary tool to observe the formation and transition of the Pt–Sn alloy phases in propane dehydrogenation. Furthermore, the relationship between catalyst deactivation and Pt–Sn alloy phases during propane dehydrogenation was discussed.

* Corresponding author. Tel.: +82 52 259 2253; fax: +82 52 259 1689.
E-mail address: ewshin@mail.ulsan.ac.kr (E.W. Shin).

0920-5861/$ – see front matter © 2010 Elsevier B.V. All rights reserved.
doi:10.1016/j.cattod.2010.10.007

Table 1
Physical properties of the reduced catalysts as measured using N_2 sorption and CO chemisoprtion.

Catalyst	Surface area[a] (m^2/g)	Pore diameter[a] (nm)	Pore volume[a] (ml/g)	Metal dispersion[b] (%)	Particle size[b] (nm)
Pt–Sn/Al	206.5	8.2	0.50	8.7	13.0
Pt–Sn/La–Al	218.4	8.6	0.69	13.4	8.5
Pt–Sn/Ce–Al	153.6	7.0	0.40	12.1	9.3
Pt–Sn/Y–Al	216.0	9.8	0.79	13.2	8.6

[a] As determined by nitrogen adsorption–desorption isotherm.
[b] As determined by CO chemisorption in a pulse system assuming CO:Pt = 1:1 and a spherical shape

2. Experimental

2.1. Catalyst preparation

Rare-earth-doped mesoporous alumina (Al) was synthesized using a modified method [22]. Typically, 6.0 g cetyl trimethyl ammonium bromide (CTAB) was added to a mixture containing 525 ml de-ionized water and 225 ml ethanol under vigorous stirring at 60 °C for 20 min. The determined amount of $La(NO_3)_3$, $Ce(NO_3)_3$, or $Y(NO_3)_3$ was added to the solution. Thirty grams of aluminum tri-sec-butoxide was added drop-wise, and 10 ml NH_4OH (28%) was added quickly to the solution. The resulting mixture was maintained at 60 °C and continually stirred for 3 h. After filtration, the product was washed with 500 ml ethanol and dried in air at 25 °C for 12 h. The product was calcined in an air flow via heating from room temperature to 550 °C at a ramping rate of 2 °C min^{-1} and holding at 550 °C for 6.0 h. Mesoporous alumina was similarly synthesized without the addition of rare earth metals and addition of NH_4OH to the solution before aluminum tri-sec-butoxide. Pt and Sn were loaded onto supports using an incipient wetness impregnation technique, and the four catalysts were designated Pt–Sn/Al, Pt–Sn/La–Al, Pt–Sn/Ce–Al, and Pt–Sn/Y–Al. In all cases, the Pt and Sn loading was 3 wt.%, and the percentages of La, Ce and Y incorporated into Al_2O_3 were 10 wt.%. All the chemicals were purchased from Sigma–Aldrich Korea (Yong-In, Kyounggi, South Korea).

2.2. Catalyst characterization

The textural properties of the catalysts were characterized using a nitrogen sorption technique (Micromeritics ASAP 2020). The samples were degassed under vacuum at 300 °C for 4 h prior to analysis and were measured at −196.15 °C using an automatic analyzer. Temperature-programmed reduction (TPR) experiments were conducted in a quartz flow reactor. The calcined catalysts were heated at 6 °C min^{-1} from room temperature to 900 °C. The reductive gas (5 vol.% H_2/N_2) was fed to the reactor at a flow rate of 10 ml min^{-1}. A BELCAT-B Catalyst Analyzer with 10 vol.% CO/He was used to determine metal dispersions using CO chemisorption. The coke content was analyzed using a thermogravimetric analyzer (TA Instruments Q50). Approximately 10 mg spent catalyst was charged into the sample pan and heated to 800 °C at a ramping rate of 20 °C min^{-1} in flowing air. X-ray diffraction (XRD) patterns were obtained on a Rigaku D/MAX-2200 powder X-ray diffractometer using a Cu Kα radiation source (λ = 0.15418 nm). Pt, PtSn, Pt_3Sn, or $PtSn_2$ phase in XRD patterns were identified by Xpowder (ver. 2004. 04. 36 Pro) and Crystal Impact (ver. 1.9e) softwares that associated with PDF-2 and IUCr/COD/AMCSD 03.07.09 data base. ^{27}Al MAS-NMR measurements were performed at room temperature on a Bruker AV3-300 with a 7.05 T magnet. For MAS NMR experiments, a 4 mm MAS probe was used with a zirconia rotor at 26.1 MHz for ^{27}Al resonance frequency. A 90° pulse length of 2.0 μs, a repetition delay of 5 s, and a spectral width of 62.5 kHz were used. The high-resolution transmission electron microscopy (HRTEM) images were obtained using a JEOL SEM-2100F. Specimens were prepared via suspension and grinding in an ethanol solution, and two drops of ethanol solution containing the ground catalyst powder were placed onto a carbon film-coated copper grid. An X-ray photoelectron spectroscopy (XPS) study of fresh and spent catalysts was conducted on a Thermo VG Scientific ESCALAB-250 instrument with an excitation source of AlK_α radiation.

2.3. Reaction test

Dehydrogenation of propane was performed in a flow reactor at atmospheric pressure. For all experiments, the catalyst (100 mg) was reduced in pure H_2 (50 ml min^{-1}) at 600 °C for 3 h followed by purging for 10 min in N_2 (100 ml min^{-1}) to remove the H_2 remaining in the reactor. The reaction mixture consisting of N_2 (100 ml min^{-1}) and C_3H_8 (30 ml min^{-1}) was fed into the reactor at 600 °C. The product was sampled at different intervals and was analyzed using gas chromatography (YOUNG LIN-Acme 6000 GC). A flame ionization detector and a 30 m × 0.53 mm HP-PLOT Al_2O_3 "KCl" capillary column were used.

3. Results and discussion

Table 1 presents the physical properties of the reduced catalysts obtained from N_2 sorption and CO chemisorption. From pore diameters, isotherms, and *t*-plots (data not shown), all of the catalysts were determined to have mesoporous structures with negligible microporosity. The incorporation of La, Ce, or Y into Al_2O_3 results in the production of more metal dispersion when compared to that of the pure Al_2O_3 support. To reveal the presences of La, Ce, or Y in the alumina framework network, the Al coordination was studied using ^{27}Al MAS-NMR, whose results are shown in Fig. 1. The spectrum of the lanthanum- and cerium-doped alumina showed three peaks at 3, 36, and 60 ppm. The first, second, and third peaks in the NMR spectra were assigned to aluminum with octahedral (O_d), pentahedral, and tetrahedral symmetries (T_d), respectively. The spectrum of alumina- and yttrium-doped alumina exhibited two peaks at 3

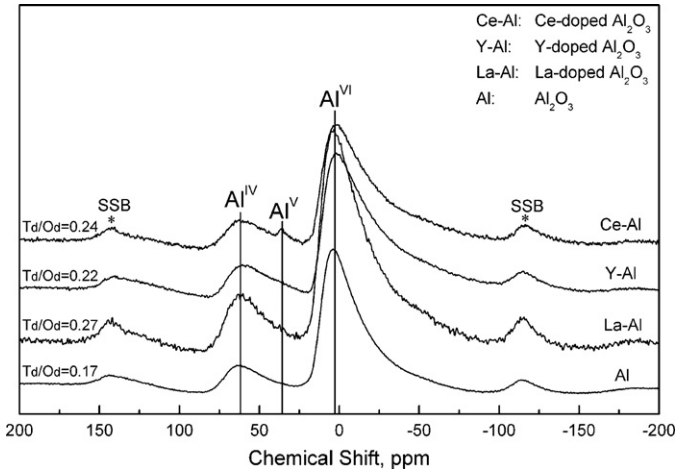

Fig. 1. ^{27}Al MAS-NMR spectra of the Al_2O_3 and La-, Ce-, Y-doped Al_2O_3 supports. SSB in the figure indicates the spinning side bands.

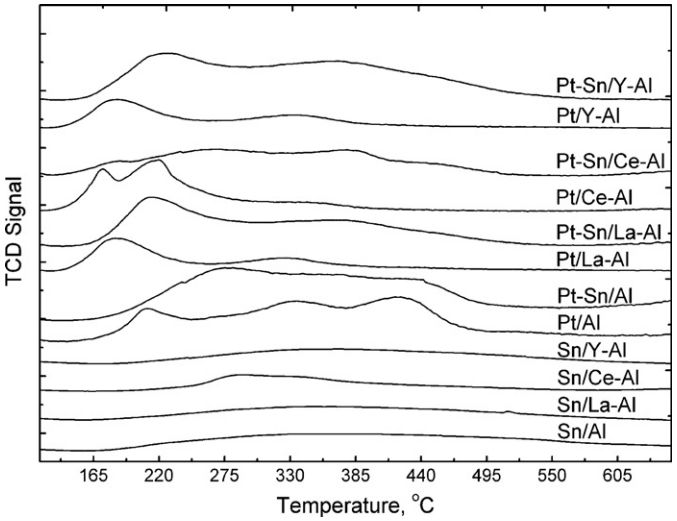

Fig. 2. TPR profiles of calcined Sn, Pt, and Pt–Sn supported on Al, La–Al, Ce–Al, and Y–Al.

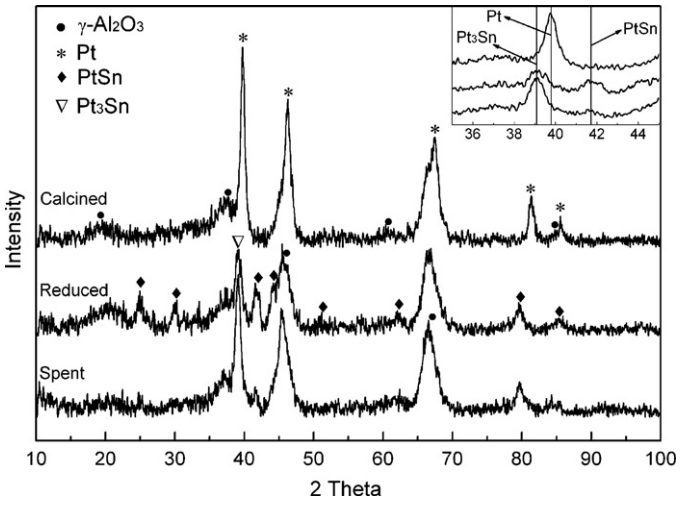

Fig. 3. XRD patterns of the calcined, reduced, and spent Pt–Sn/Al catalysts.

and 60 ppm corresponding to octahedral and tetrahedral symmetries, respectively. Moreover, the T_d/O_d ratios in the La–Al and Ce-Al were relatively higher than those in the Y–Al and pure alumina. This indicates that the numbers of sites with tetrahedral and pentahedral symmetries increased with La- and Ce–doping, and a certain portion of La, Ce, or Y was integrated into the alumina framework.

Fig. 2 presents the TPR profiles of all calcined Sn, Pt, and Pt–Sn/supports catalysts. The TPR profile of Pt/Al showed at least three unresolved peaks at 210, 335, and 423 °C that indicate differences in the interactions between the Pt species and the Al_2O_3 support. These peaks were attributed to different oxychlorinated Pt species formed after impregnation of the chloroplatinic acid into Al_2O_3 support and thermal treatment processes, such as drying and calcinations [23,24]. The TPR profile of the Pt/Ce–Al exhibited two main peaks at 172 and 220 °C and one small peak at 350 °C, dramatically different from that of the Pt/Al sample. This observation can be explained by the Pt-ceria interaction leading to the easier reduction of ceria by hydrogen spillover from Pt to cerium oxide. Furthermore, the presence of ceria promotes the reductions of Pt species due to preferential interaction of Pt with ceria compared to that of alumina [4,25]. The TPR profiles of Pt/La–Al and Pt/Y–Al exhibited similar behaviors that consisted of two reduction peaks that shifted to a lower reduction temperature comparable to that of Pt/Al. Both of the catalysts had the same first reduction peak at 180 °C with second reduction peaks at 325 and 333 °C on the Pt/La–Al and Pt/Y–Al, respectively. This observation suggests that the addition of La and Y into Al_2O_3 results in a decrease in reduction temperatures of the platinum species. This observation is consistent with a previous report suggesting that La promotes the reduction of the Pt species via an electron pushing effect [26]. The shift in the reduction peaks of Pt toward a lower temperature was also observed on the SiO_2 support with the addition of rare earth oxides [27].

The reduction peaks in the TPR profiles of the Pt–Sn/supports consistently shifted to higher reduction temperatures comparable to that in TPR profiles of Pt/supports. This TPR profile was very different from that corresponding to the sum of the TPR profile from Pt/supports and Sn/supports; consequently, this is a sign of co-reduction of Pt–Sn species. Moreover, several Pt–Sn alloys on the reduced Pt–Sn/supports were revealed in the XRD patterns. The TPR profiles of Sn/Al, Sn/La–Al, and Sn/Y–Al did not demonstrate a well-defined reduction temperature and showed very small hydrogen consumptions with broad peaks of low intensity. Alternatively, the TPR profile of Sn/Ce–Al exhibited two unresolved reduction zones; the first peak at 285 °C can be attributed to the reduction of superficial CeO_2, and the second peak at 342 °C can be assigned to the formation of non-stoichiometric cerium oxide [28]. Tin–alumina interactions hindered the reduction of the Sn species to metallic Sn, and the presence of Pt induced the reduction of the tin species to metallic tin via hydrogen-activated Pt with intimate contact between the Pt and Sn (II, IV) [29].

The Pt–Sn system existed in the following phases: Pt_3Sn, PtSn, Pt_2Sn_3, $PtSn_2$, and $PtSn_4$ [30]. The one-to-one atomic composition (PtSn) was the most frequently detected phase via several techniques, although all types of Pt–Sn alloys are possible. The influence of the Al_2O_3 surface area and the atomic ratio (1–8) of Pt/Sn on the type of Pt–Sn alloy phase has been previously studied [31], demonstrating that only one type of Pt–Sn alloy (Pt:Sn = 1:1) was observed with varying surface area and Pt/Sn atomic ratio. However, the various Pt–Sn alloy phases, such as Pt_3Sn, PtSn and $PtSn_2$ on the Al_2O_3 support, have been detected via XRD in other reports [15,32]. Investigation of the Pt–Sn alloy system with various Pt/Sn atomic ratios (0.2–1.78) on the $ZnAl_2O_4$ support has also been examined, and it was found that the most stable alloy was PtSn with a trace amount of Pt_2Sn_3 [33]. It is worth noting that the formation of the Pt–Sn alloy type on supports should be different from that on the unsupported Pt–Sn alloy, as the same Pt/Sn atomic ratios were compared.

XRD patterns corresponding to Pt–Sn/Al, Pt–Sn/La–Al, Pt–Sn/Ce–Al, and Pt–Sn/Y–Al catalysts are shown in Figs. 3–6, respectively. Pt (PDF no.: 00-004-0802) and γ-Al_2O_3 (PDF no.: 00-029-0063) phases were detected on all of the calcined catalysts, and the CeO_2 phase (PDF no.: 00-034-0394) was identified on the calcined, reduced, and spent Pt–Sn/Ce–Al catalyst. These observations are consistent with a previous report in which $H_2PtCl_6{\cdot}6H_2O$ precursor decomposed into Pt metal and other products above 510 °C in He or air [34]; this decomposition temperature was lower than the calcination temperature (550 °C) in our experiment, in which Pt_3Sn (PDF no.: 00-035-1360) and PtSn (AMCSD no.: 99-101-0886) alloys were formed on the reduced Pt–Sn/Al catalyst, and the Pt_3Sn phase became predominant after the reaction (Fig. 3). PtSn alloy formed on the reduced Pt–Sn/La–Al catalyst, and the Pt_3Sn phase appeared after the reaction, while a significant amount of PtSn phase remained. The $PtSn_2$ phase (AMCSD no.: 99-101-1008) was formed on the reduced Pt–Sn/Ce–Al catalyst, and this phase remained dominant after the reaction although there was a transformation to Pt_3Sn. $PtSn_2$ and PtSn phases were formed on the reduced Pt–Sn/Y–Al catalyst, and $PtSn_2$ nearly transformed to Pt_3Sn after the reaction. In summary, Pt–Sn alloy phases were detected using XRD measurements, and the Pt–Sn

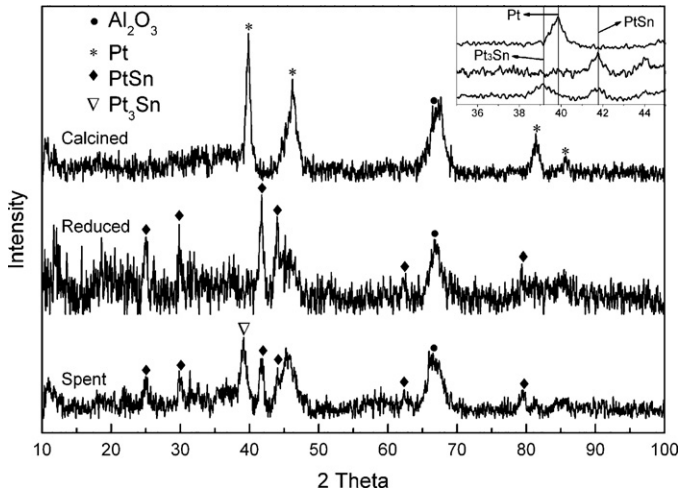

Fig. 4. XRD patterns of the calcined, reduced, and spent Pt–Sn/La–Al catalysts.

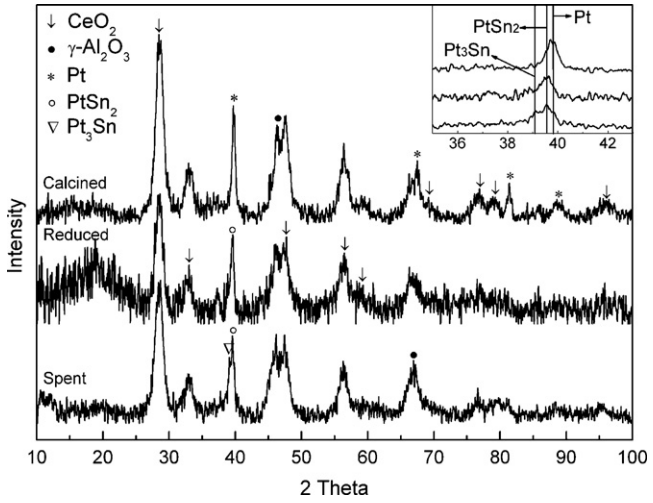

Fig. 5. XRD patterns of the calcined, reduced, and spent Pt–Sn/Ce–Al catalysts.

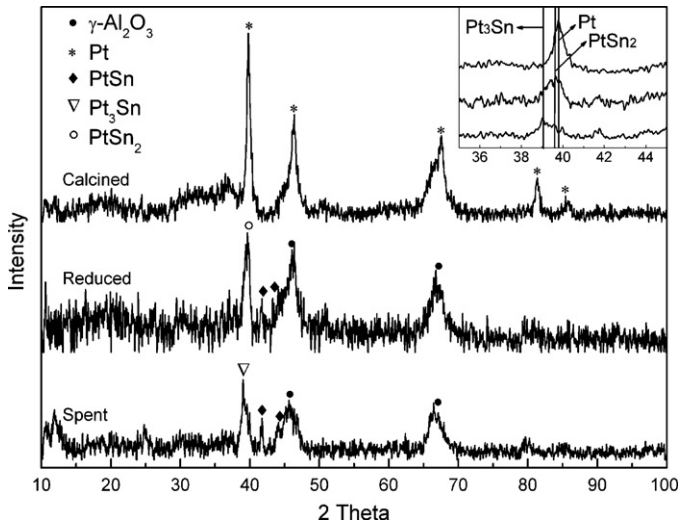

Fig. 6. XRD patterns of the calcined, reduced, and spent Pt–Sn/Y–Al catalysts.

alloy phases were transformed to Pt_3Sn during the reaction. However, there was a different behavior in the Pt–Sn alloy phase transition during the reaction, depending on the catalyst. For the Pt–Sn/La–Al and Pt–Sn/Ce–Al, the PtSn or $PtSn_2$ alloy was stable and was still present after the reaction, whereas the Pt_3Sn alloy was predominant for Pt–Sn/Y–Al and Pt–Sn/Al.

Fig. 7 shows the HRTEM images of the reduced and spent Pt–Sn/support catalysts. Larger metal particles were observed in the spent Pt–Sn/support catalysts than were seen in the reduced Pt–Sn/support catalysts, indicating that the sintering process occurred during the reaction, consistent with XPS measurements showing the loss of Pt dispersion on the spent catalysts. Moreover, the platinum-rich Pt_3Sn alloy was detected on all of the spent Pt–Sn/support catalysts using XRD, and sintering occurred via agglomeration between the unalloyed Pt and PtSn or $PtSn_2$ alloy to produce the Pt_3Sn alloy. However, no inference within the sintering mechanism could be derived from the particle size distribution [35].

XPS analysis results of the reduced and spent catalysts are provided in Table 2. Based on the Pt/Al ratio, the addition of the rare earth metals into Al_2O_3 improved Pt dispersion, consistent with CO chemisorption data. Alternatively, the Pt/Al XPS atomic ratios decreased for all of the spent catalysts. A significant decrease in Pt dispersion was observed on both the Pt–Sn/Y–Al and Pt–Sn/Al catalysts after the reaction, while the Pt–Sn/La–Al and Pt–Sn/Ce–Al catalysts exhibited only a small decrease in Pt dispersion. The attenuation of the Pt signal in XPS caused by the coke coverage was an additional factor that contributed to the overall decrease in Pt dispersion measured using XPS. The binding energies of La $3d_{5/2}$ at 835.27 over the reduced Pt–Sn/La–Al catalyst and of Y $3d_{5/2}$ at 158.14 eV on the reduced Pt–Sn/Y–Al catalyst indicated the dispersed phases of lanthanum and yttrium oxide rather than bulk R_2O_3 or $RAlO_3$ with lower binding energies (R = La, Y) [36]. The Ce $3d_{5/2}$ XPS consists of a complicated spectrum with overlapping peaks. The peak at the binding energy of 916 eV (u‴) is normally used as the marker to detect the presence of the Ce^{4+} state and is assigned to $4f^0$ orbital transitions. Based on the percentage of the u‴ component, the ratio of the CeO_2 phase to the total oxide form of cerium can be estimated [37]. The u‴ components were 12% and 10% of the reduced and spent Pt–Sn/Ce–Al, respectively, corresponding to 80% CeO_2 in the former and 70% CeO_2 in the latter. The decrease in CeO_2 percentage after the reaction was probably due to the reduction roles of the hydrogen gas and coke generated during the reaction. This observation agrees with the XRD patterns of the reduced and spent Pt–Sn/Ce–Al catalysts which show the formation of a separate CeO_2 phase.

In propane dehydrogenation over Pt–Sn supported catalysts, propene (target product) and other products (CH_4, C_2H_6, C_2H_4) were detected by FID while C4+ products were not detected or under limit of detection of detector despite of longer retention time. Therefore, it was concluded that by-products were mainly CH_4, C_2H_6, C_2H_4, H_2, and coke. Carbon balance was verified for each experiment following the below equation:

$$\text{Carbon balance} = \frac{3n(C_3H_8)_{in}}{n(CH_4)_{out}+2n(C_2H_6)_{out}+2n(C_2H_4)_{out}+3n(C_3H_8)_{out}+3n(C_3H_6)_{out}}$$

where $n(C_3H_8)_{in}$ was the numbers of moles of propane from inlet; $n(C_xH_y)_{out}$ was the numbers of moles of products from outlet. The values of carbon balance in the calculation were usually higher than unit because coke containing rich-carbon structure remained on catalysts during the reactions.

Fig. 8 exhibits the catalytic conversion of propane to propene on various Pt–Sn/supports catalysts; the deactivation parameters and coke contents are summarized in Table 3. TGA analysis provided the following order of catalyst with regard to coke content: Pt–Sn/Y–Al > Pt–Sn/Al > Pt–Sn/Ce–Al > Pt–Sn/La–Al, which correlated well with the order of deactivation parameters. Com-

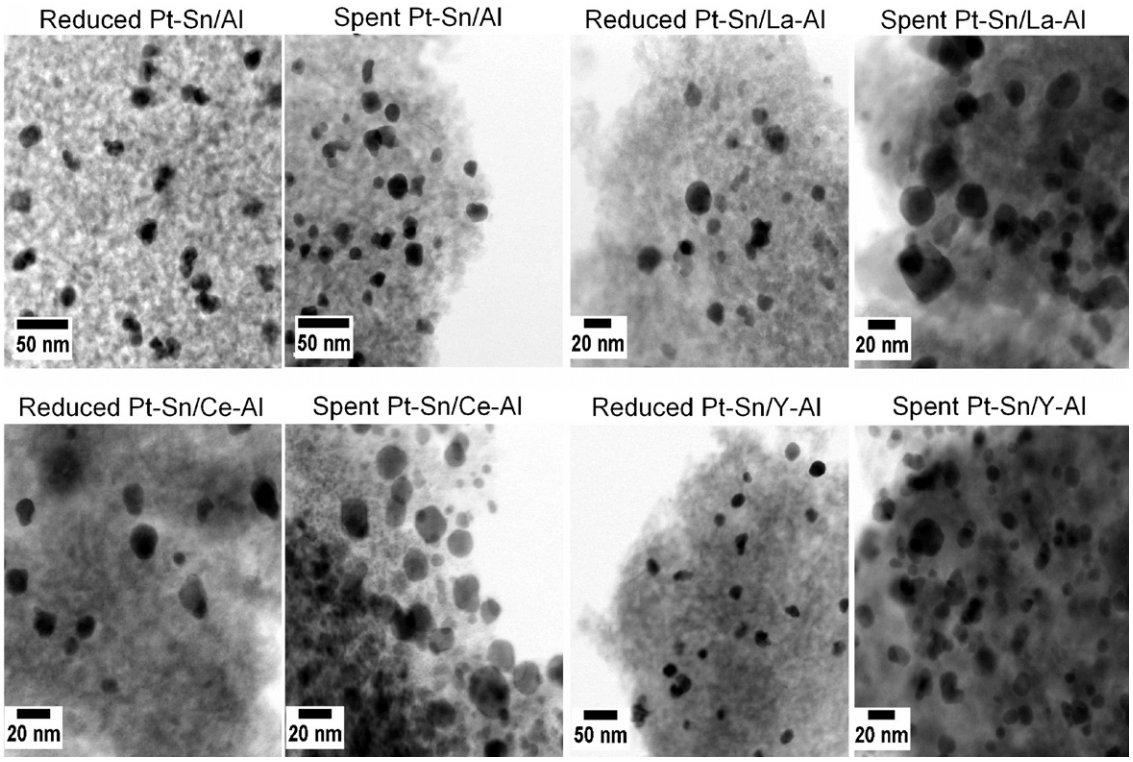

Fig. 7. HRTEM images of the reduced and spent Pt–Sn/supports catalysts.

Table 2
Binding energies and surface compositions of reduced (red) and spent (rxn) catalysts as measured by XPS.

Catalyst	Binding energy (eV)					Atomic ratio (atom/atom)				
	$Pt^{(0)}$ $4f_{7/2}$	$Sn^{(0)}$ $3d_{5/2}$	La $3d_{5/2}$	Ce $3d_{5/2}$	Y $3d_{5/2}$	Pt/Al	Sn/Pt	Ce/Al	La/Al	Y/Al
Pt–Sn/Al (red)	71.70	485.53	–	–	–	0.0042	3.35	–	–	–
Pt–Sn/Al (rxn)	71.71	485.22	–	–	–	0.0021	7.25	–	0.026	–
Pt–Sn/La–Al (red)	71.69	485.59	835.27	–	–	0.0065	2.31	–	0.025	–
Pt–Sn/La–Al (rxn)	71.70	485.77	835.56	–	–	0.0058	2.75	–	–	–
Pt–Sn/Ce–Al (red)	71.68	485.66	–	u, u′, u″, u‴v, v′, v″, v‴	–	0.011	3.04	0.028	–	–
Pt–Sn/Ce–Al (rxn)	71.74	485.49	–	u, u′, u″, u‴v, v′, v″, v‴	–	0.0080	4.05	0.022	–	–
Pt–Sn/Y–Al (red)	71.70	485.63	–	–	158.14	0.013	1.11	–	–	0.029
Pt–Sn/Y–Al (rxn)	71.69	485.66	–	–	158.06	0.0025	6.71	–	–	0.026

(–) not detected.

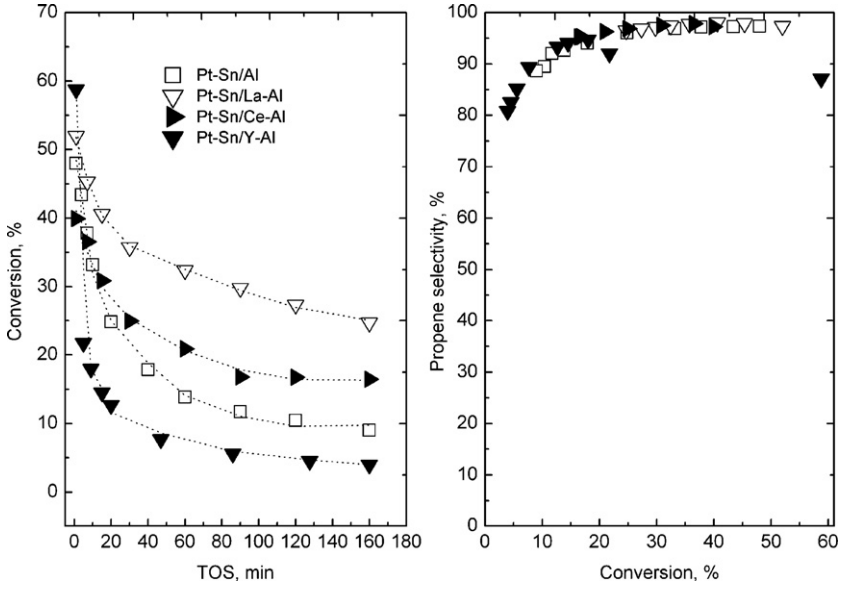

Fig. 8. Catalytic performances of the catalysts in propane dehydrogenation. (a) Conversion vs. time on stream, and (b) propene selectivity vs. conversion.

Table 3
Deactivation parameters and coke contents as determined by TGA.

Catalyst	Pt–Sn/Al	Pt–Sn/La–Al	Pt–Sn/Ce–Al	Pt–Sn/Y–Al
Deactivation parameter (X_f/X_0)[a]	0.19	0.48	0.41	0.07
Coke content (wt.%)	7.7	3.9	4.5	9.7

[a] X_f and X_0 are the final and initial propane conversions, respectively.

pared to the catalytic performance of Pt–Sn/Al, Pt–Sn/La–Al and Pt–Sn/Ce–Al showed better tolerance to catalyst deactivation and a lower coke amount, whereas Pt–Sn/Y–Al was deactivated faster. The final conversion of the catalysts also follows the same trend: Pt–Sn/Y–Al < Pt–Sn/Al < Pt–Sn/Ce–Al < Pt–Sn/La–Al. However, in the plot of selectivity vs. conversion, all of the points seem to be linear, implying that there was no difference in the catalyst preference to propene selectivity.

These observations were believed to be due to the transformation of the Pt–Sn alloy and the loss of Pt dispersion during the reaction, as measured by XRD and XPS. According to literature [10,38,39], catalyst deactivation was due to low mobility of coke. Sn acted like a scavenger to keep Pt sites clean from coke deposits by spillover of coke precursors from active sites to the support. The catalyst deactivation by coke deposits depends on coke location that relates to coke mobility; the catalyst deactivation occurs when coke locates directly only on the active sites not the support (herein, pore plugging by coke is excluded from coking behavior because of the short reaction time). Coke mobility was usually verified by the temperature-programmed oxidation. The addition of Sn into Pt increased the mobility of coke (coke moved to and located on support) and therefore oxidation temperature of coke was shifted to higher temperature because oxidation reaction was not catalyzed by Pt [10,38,39]. In this sense, we proposed that the mobility of coke precursors was lower on Pt_3Sn than that on other tin-rich Pt–Sn alloys (PtSn, $PtSn_2$). To our knowledge, the influence of each Pt–Sn alloy on mobility of coke has not been studied yet. Instead, it has been reported that the type of Pt–Sn alloy remarkably influenced the desorption possibility for pi-bond molecules, and temperature-programmed desorption experiments revealed that the desorption of pi-bond molecules onto unsupported PtSn and $PtSn_2$ alloys becomes progressively easier than that on unsupported Pt_3Sn alloy [1]. This factor contributes to the overall fast deactivations of both Pt–Sn/Al and Pt–Sn/Y–Al catalysts because Pt_3Sn became a dominant phase during the reaction, and therefore there was a strong interaction between Pt_3Sn and the sp^2 carbon-containing coke. Therefore, the mobility of coke was different on different Pt–Sn alloys, indicating a significant role in the overall catalytic deactivation.

4. Conclusions

Influences of La-, Ce-, and Y-doped Al_2O_3 on the formation, stability, and catalytic performance of Pt–Sn alloys in propane dehydrogenation were investigated. Diverse characterizations such as ^{27}Al MAS-NMR, XRD, and XPS revealed that a portion of the La, Ce, and Y were incorporated into the Al_2O_3 framework; La and Y also formed a dispersed phase, whereas Ce constituted as a separate phase of CeO_2 on Al_2O_3. Moreover, La-, Ce-, and Y-doped Al_2O_3 increased the Pt dispersion and decreased the reduction temperature of the Pt–Sn species comparable to those on Al_2O_3, confirmed via CO chemisorption, XPS, and TPR. In catalytic tests, the Pt–Sn/La and Pt–Sn/Ce–Al catalysts exhibited the best catalytic performances and stabilities because of the low coke content, high stability of Pt–Sn alloy phases, and small loss of Pt dispersion. The XRD measurements identified the formation of Pt–Sn alloy phases after reduction and the phase transition during the reaction. Pt_3Sn and PtSn alloys were formed on the reduced Pt–Sn/Al catalyst, while the PtSn alloy was transformed predominantly into Pt_3Sn alloy via reaction with the Pt–Sn/Al catalyst. Alternatively, only the PtSn alloy was formed on the reduced Pt–Sn/La–Al catalyst, and it exhibited a significant stability even though a new phase of Pt_3Sn appeared on the spent Pt–Sn/La–Al catalyst. A $PtSn_2$ alloy was formed on the reduced Pt–Sn/Ce–Al and Pt–Sn/Y–Al catalysts, and both $PtSn_2$ and Pt_3Sn alloys coexisted on the spent Pt–Sn/Ce–Al and Pt–Sn/Y–Al catalysts; however, the $PtSn_2$ phase was more stable on the spent Pt–Sn/Ce–Al than it was on the spent Pt–Sn/Y–Al, on which it nearly transformed into the Pt_3Sn phase. The transition to the Pt_3Sn alloy during the reaction in the Pt–Sn bimetallic system was responsible for a weak tolerance for catalyst deactivation.

Acknowledgements

This work was supported by the Energy Efficiency & Resources program of the Korea Institute of Energy Technology Evaluation and Planning (KETEP) grant funded by the Korea government Ministry of Knowledge Economy (no. 2007MCC24P0230202009).

References

[1] H. Verbeek, W.M.H. Sachtler, J. Catal. 42 (1976) 257.
[2] G. Meitzner, G.H. Via, F.W. Lytle, S.C. Fung, J.H. Sinfelt, J. Phys. Chem. 92 (1988) 2925.
[3] M.P. Lobera, C. Teĭllez, J. Herguido, M. Meneĭndez, Ind. Eng. Chem. Res. 47 (2008) 9314.
[4] C. Yu, Q. Ge, H. Xu, W. Li, Appl. Catal. A 315 (2006) 58.
[5] G. Del Angel, A. Bonilla, Y. Peña, J. Navarrete, J.L.G. Fierro, D.R. Acosta, J. Catal. 219 (2003) 63.
[6] M.L. Casella, G.J. Siri, G.F. Santori, O.A. Ferretti, M.M. Ramirez-Corredores, Langmuir 16 (2000) 5639.
[7] C. Yu, H. Xu, Q. Ge, W. Li, J. Mol. Catal. A 266 (2007) 80.
[8] G.J. Siri, G.R. Bertolini, M.L. Casella, O.A. Ferretti, Mater. Lett. 59 (2005) 2319.
[9] N. Al-Yassir, R. Le Van Mao, Appl. Catal. A 317 (2007) 275.
[10] C.L. Padró, S.R. de Miguel, A.A. Castro, O.A. Scelza, C.H. Bartholomew, G.A. Fuentes, Stud. Surf. Sci. Catal. 111 (1997) 191.
[11] Y. Wang, Y. Wang, S. Wang, X. Guo, S.-M. Zhang, W.-P. Huang, S. Wu, Catal. Lett. 132 (2009) 472.
[12] J.M. Hill, R.D. Cortright, J.A. Dumesic, Appl. Catal. A 168 (1998) 9.
[13] J. Llorca, N. Homs, J. León, J. Sales, J.L.G. Fierro, P. Ramirez de la Piscina, Appl. Catal. A 189 (1999) 77.
[14] S.M. Stagg, C.A. Querini, W.E. Alvarez, D.E. Resasco, J. Catal. 168 (1997) 75.
[15] C. Kappenstein, M. Guérin, K. Lázár, K. Matusek, Z. Paál, J. Chem. Soc., Faraday Trans. 94 (1998) 2463.
[16] Z. Huang, J.R. Fryer, C. Park, D. Stirling, G. Webb, J. Catal. 159 (1996) 340.
[17] J. Llorca, P.R. Delapiscina, J.L.G. Fierro, J. Sales, N. Homs, J. Catal. 156 (1995) 139.
[18] C. Audo, J.F. Lambert, M. Che, B. Didillon, Catal. Today 65 (2001) 157.
[19] G.J. Siri, M.L. Casella, G.F. Santori, O.A. Ferretti, Ind. Eng. Chem. Res. 36 (1997) 4821.
[20] J. Llorca, P.R. de la Piscina, J.-L.G. Fierro, J. Sales, N. Homs, J. Mol. Catal. A 118 (1997) 101.
[21] H. Davis Burtron, Selectivity in Catalysis, American Chemical Society, Washington, DC, 1993, p. 109.
[22] M.W.T.B.H.S.W. Deng, Adv. Funct. Mater. 13 (2003) 61.
[23] H. Lieske, G. Lietz, H. Spindler, J. Völter, J. Catal 81 (1983) 8.
[24] G. Lietz, H. Lieske, H. Spindler, W. Hanke, J. Völter, J. Catal. 81 (1983) 17.
[25] V. Pitchon, J.F. Zins, L. Hilaire, G. Maire, React. Kinet. Catal. Lett. 59 (1996) 203.
[26] Y. Zhang, Y. Zhou, H. Liu, Y. Wang, Y. Xu, P. Wu, Appl. Catal. A 333 (2007) 202.
[27] F. Wang, G. Lu, J. Power Sources 181 (2008) 120.
[28] J.Z. Shyu, W.H. Weber, H.S. Gandhi, J. Phys. Chem. 92 (1988) 4964.
[29] H. Lieske, J. Völter, J. Catal. 90 (1984) 96.
[30] P. Anres, M. Gaune-Escard, J.P. Bros, E. Hayer, J. Alloys Compd. 280 (1998) 158.
[31] R. Srinivasan, R.J. Angelis, B.H. Davis, Catal. Lett. 4 (1990) 303.

[32] M. Tasbihi, F. Feyzi, M.A. Amlashi, A.Z. Abdullah, A.R. Mohamed, Fuel Process. Technol. 88 (2007) 883.
[33] N.A. Pakhomov, R.A. Buyanov, E.M. Moroz, E.N. Yurchenko, A.P. Chernyshev, N.A. Zaitseva, G.R. Kotelnikov, React. Kinet. Catal. Lett. 14 (1980) 329.
[34] A.E. Schweizer, G.T. Kerr, Inorg. Chem. 17 (1978) 2326.
[35] A.K. Datye, Q. Xu, K.C. Kharas, J.M. McCarty, Catal. Today 111 (2006) 59.
[36] J.S. Church, N.W. Cant, D.L. Trimm, Appl. Catal. A 101 (1993) 105.
[37] J.Z. Shyu, K. Otto, J. Catal. 115 (1989) 16.
[38] L. Liwu, Z. Tao, Z. Jingling, X. Zhusheng, Appl. Catal. 67 (1990) 11.
[39] Y. Zhang, Y. Zhou, A. Qiu, Y. Wang, Y. Xu, P. Wu, Catal. Commun. 7 (2006) 860.